Journal of the Indian Society of Remote Sensing (December 2020) 48(12):1767–1785
https://doi.org/10.1007/s12524-020-01202-8

RESEARCH ARTICLE

Monitoring of Land Use and Land Cover Change Detection Using Multi-temporal Remote Sensing and Time Series Analysis of Qena-Luxor Governorates (QLGs), Egypt

Mostafa Kamel[1]

Received: 7 July 2020 / Accepted: 5 October 2020 / Published online: 13 October 2020

Abstract
In recent years, rapid land use land cover (LULC) changes have continuously taken place in many regions all over the world as a result of human activities. In the present study, the changes in LULC were analyzed by means of multi-temporal remote sensing of Qena-Luxor Governorates in Egypt between 1984 and 2018. In order to map and monitor the land use land cover changes, several remotely sensed data were applied to create multi-maps using (1) the normalized difference vegetation index and (2) supervised classification of Landsat images using field chick and accuracy assessment, including field verification and Google Earth Professional. Therefore, the lands in the study area can be classified as follows: (1) agricultural lands, (2) built-up areas, (3) water bodies, (4) reclaimed lands, and (5) desert lands. The results indicate that agricultural lands grew from an average of 1238.7 km^2 (9.8%) in 1984 to 1707.04 km^2 (13.40%) in 2018 and urban lands increased from 345.2 km^2 (2.7%) in 1984 to 445.28 km^2 (3.5%) in 2019. Furthermore, the reclaimed lands increased approximately from 4379.7 km^2 in 1984 (i.e., 34.4% of the total study area) to 4521.05 km^2 in 2000 (35.507%). However, this class was followed by a marked decline to 4373.51 km^2 (34.35%) between 2000 and 2010 and then increased to approximately 4442 km^2 (34.89%) between 2010 and 2018. Desert lands (limestone plateau and some lowland desert fringes) decreased from 6635.4 km^2 (52.2%) to 6003.5 km^2 (47.15%). The results showed that the overall accuracy of the supervised classification of Landsat satellite images ranges from 87 to 92.5% while kappa statistics were from 0.83 to 90.

Keywords Land use/land cover · Change detection · Landsat data · Accuracy assessment · Qena-Luxor governorates · Egypt

Introduction

Land use land cover (LULC) changes in the world are directly proportional to environmental changes, as well as human interaction with lands. Therefore, studying and analyzing environmental changes are a vital requirement for understanding LULC changes. The remotely sensed data is an important effective tool for LULC mapping in different periods of time. Several recent works were published to show the ability of satellite technology utilization, image classification, and processing techniques to detect LULC changes in regional, national, continental, and even global levels of large-area data analyses (Chen et al. 2014; Leinenkugel et al. 2019; Pflugmacher et al. 2019). Mondal et al. (2016) described the LULC pattern as a dynamic process.

Change detection is significant for the study of land degradation resulting from environmental processes and management with implications for biodiversity. Remotely sensed data covering the earth's surface has detected a number of regional and global changes in LULC. Several authors have argued that this is primarily due to operations such as (1) agricultural intensification, (2) globalization tropical deforestation, (3) socioeconomic aspects, (4) biophysical attributes, and (5) urbanization (Lambin, 1997; Lambin et al. 2001; Veldkamp and Lambin, 2001; Zeng et al. 2008; Duraisamy et al. 2018; Dash et al. 2018).

✉ Mostafa Kamel
Mostafa.kamel@azhar.edu.eg; mos_kamel80@yahoo.com

[1] Geology Department, Faculty of Science, Al-Azhar University, Assiut 71516, Egypt

Generally, what the rate and extent of land cover changes are and how we determine these changes that have occurred in the area during the time period between 1984 and 2018 are the main scientific research questions herein.

In fact, sensors of Landsat platforms with high spatial–temporal-spectral resolutions are one of the most important factors for LULC change detection using several methods (supervised classification, NDVI, and NDBI). GIS is an important geoenvironmental system used as powerful tools to capture, store, check, pan-sharp, process, interpret, and display data. Remotely sensed data and GIS integrated were applied for detecting, mapping, and monitoring LULC changes, as well as for water quality mapping and monitoring (Joshi et al. 2002; Rebelo et al. 2009; Durga Rao et al. 2009).

Egypt is one of the most important countries in Africa; it covers about 1,002,450 km^2 representing about 3.32% of Africa's total area. Egypt is one of the most populous countries in Africa and the Middle East, with an estimated population of 102,150,654 million in 2020, where it represents 1.31% of the world population percentage, it ranks the 14th, its population growth rate is 1.94% (54th), and its population density is 102/km^2 (111th) (world population review 2020).

Socially, the Egyptian citizens live in the Delta of Nile Valley and along the two Nile River banks, which represent 10% of the land of Egypt. On the other hand, a small number of populations live in the desert lands of Egypt. The existence of reclamation projects in the desert regions permits us to execute urban, agricultural, and economic projects. Therefore, the changes of the earth surface in the arid regions should be studied to detect the importance of land use task.

The study area includes Qena and Luxor Governorates; both of them were one governorate before but they were separated in 2009. Qena Governorate includes 9 provinces. It covers an area of about 10,798 km^2. Luxor is a modern name for the ancient city of Thebes, and it was important because it was considered as the great capital of Upper Egypt in the past. It is called the "world's greatest open-air museum." It is unique because it contains one-third of the world's monuments as Karnack and Luxor temples; therefore, thousands of tourists from all around the world arrive annually to visit these monuments. Seven provinces belong to Luxor Governorate. It covers an area of about 2959.6 km^2.

QLGs are suited under arid and semiarid climatic conditions. The environmental changes almost happened due to human activities or natural forces as LULC changes (Zhou et al. 2008). Alphan et al. (2009) stated that the assessment of ecosystem and environmental conditions basically depends on the valuable information related to land cover changes at different dates. Rawat and Kumar (2015) reported that the land cover concept means the physical materials that occur on the earth's surface.

Information about LULC changes is very important to detect and understand the management of natural resources (Iqbal and Khan 2014; Kanta Kumar and Neelamsetti 2015; Lin et al. 2015).

In the present work, many techniques are applied to detect LULC changes, such as post-supervised classification of remotely sensed images, NDVI, and GIS technique.

Space science techniques as remote sensing can provide useful land cover/land use data with lower effort and cost than traditional field observations (Szuster et al. 2011). Many Landsat satellite versions have provided high spatial–temporal resolution imagery data for specific land science authors to monitor and map earth surface changes since the 1970s (Hansen and Loveland 2012).

Many scientific studies were published to report the importance of LULC change detection to use in sustainable resource management; they utilized high spatial–temporal resolution of Landsat imagery for large-scale approaches (Nitin et al. 2014; Zhiliang et al. 2015; Rawat and Kumar, 2015; Halmy et al. 2015, Amna et al. 2015; Liu et al. 2015; Yuanbin et al. 2016; Wang et al. 2017; Mack et al. 2017; Close et al. 2018; Leinenkugel et al. 2019; Massetti and Gil 2020, Nguyen et al. 2020).

In Egypt, many researchers worked on LULC change detection (Yin et al. 2005; Youssef and Ghallab 2007; Abdalla and Moubark 2018; Mohamed and El-Raey 2019; Allama et al. 2019). Shalaby and Tateishi (2007) classified land use in the Northern Egyptian coastal zone into eight classes using the supervised classification method of Landsat 4 and 5 images. In the Western Nile Delta, the hybrid post-classification of multi-temporal-spectral satellite images and NDVI methods were applied to detect LULC changes (Bakr et al. 2010; Abd El-kawy et al. 2011). Kamel and Abu El Ella (2016) studied the desert fringes along the two banks of the Nile River in the area between Assiut and Sohag Governorates for LULC change detection during three periods (1984, 2000, and 2013).

Egyptian desert fringes covered by the new and old alluvial floodplain of the Nile Valley represent the promising desert areas for land reclamation. Recently, the Egyptian government proposed a big project to construct new urban and agricultural communities along the two side desert fringes of the River Nile, the project called "1.5 Million Acres."

There should be suitable areas for the horizontal expansion in agricultural and urban communities to provide the necessities of life. Therefore, the Egyptian government is strongly interested in land reclamation in desert lowlands (reclaimed lands). Most of the lowlands in the current area such as the southern part of Wadi Qena, southwest of Qena, and east and west of Luxor

Governorate are within the Egyptian national project to reclaim 1.5 million acres.

Gaber et al. (2020) studied the west Qena area; they reported that remote sensing, geoelectric resistivity data, and the aeromagnetic techniques together were effective in exploring the groundwater potentiality. The area of southwest Qena Governorate is characterized by very high recharge potentiality and it has a thick reservoir; this reservoir is suitable for different uses (Gaber et al. 2020). Likewise, there are many desert fringe areas suitable for agricultural and urban expansion if hydrogeological studies are available.

Purpose of the Study

The aim of this paper is to capture and detect the LULC changes in Qena-Luxor Governorates (QLGs) in Upper Egypt using the supervised classification of remotely sensed data and NDVI approaches within the GIS environment during the period from 1984 to 2018. Moreover, the present study aims to answer the question of how land use has been changed in the period between 1984 and 2018.

The Study area Description

The study area includes two governorates: Qena in the north and Luxor in the south. In Qena Governorate, the population is increasing significantly, where the total population increased from 1,286.860 in 1984 to 3.224,981 in 2018. On the other hand, the population numbers of Luxor Governorate increased from 484,132 in 2010 to 1.270.021 in 2018 (Central Agency for Public Mobilization and Statistics). The current area consists of 16 municipal provinces. It is located between 25°15′–26°15′N and 32°00′–33°00′E, covering a total area of 12,732.600 km^2 (Fig. 1).

Geologically, the surface of the QLG area is covered by Phanerozoic rocks ranging in age from Late Cretaceous to Quaternary (Fig. 2). Upper Cretaceous rocks represent the oldest rock units by Qusseir, Duwi, and Dakhla Formations, while Kurkur, Tarawan, and Esna Formations belong to the Paleocene age. In the study area, Eocene is represented by Thebes Formation. Most of the current study covered the Quaternary deposits, which are represented by Muneiha Formation (Pliocene), Issawia Formation, Qena Formation, Fanglomerates (Pleistocene), Wadi deposits, and Nile silt (Holocene) (Said 1981; Faris et al. 1985; Conoco 1987; Issawi et al. 2009).

Geomorphologically, the study area is categorized into three main geomorphic units, based on the available Landsat 8 images, Shuttle Radar Topography Mission (SRTM) DEM (30 m), and topographic maps (scale 1:50,000). The three main geomorphic units are as follows: (1) flood plain deposits (cultivated land), (2) the old alluvial plain, and (3) the calcareous limestone plateau.

The most important factors associated with choosing suitable regions for reclamation to establish new urban communities are the following: good soils, appropriate climate conditions, topographic attitude, availability of freshwater, whether surface or groundwater, and establishment of roads to reach these areas. Accordingly, from previous and current studies, the study area is considered one of the most promising areas in this field. The surface soil map is redigitized and identified based on the soil map generated by the FAO (https://esdac.jrc.ec.europa.eu) (Fig. 3). The soil map helps us to detect and know various soil types covered in the present study. It also helps us to select the most suitable place for reclamation. Arc map GIS integrated with Google Earth pro 8.0v has been used to create a base map of the current area.

The area under consideration is characterized by extremely hot summer and cold winter with very low and erratic rainfall and high evaporation rates. The available meteorological data presented in this study cover the years from 1913 to 1996 (Meteorological Authority of Egypt 1996). The mean annual rainfall (mm/year) in the study area ranges from 0.7 to 4.38, which was obtained by the PERSIANN-Cloud Classification System (PERSIANN-CCS) and the Tropical Rainfall Measuring Mission (TRMM) rainfall data covering the period from 1998 to 2018 (https://gpm.nasa.gov/trmm and https://chrsdata.eng.uci.edu/). Generally, the climatic data revealed that the average temperature ranges from 5 °C in winter to 45 °C in summer whereas the average minimum temperature ranges from 5 to 14 °C.

Materials and Methods

Data Collection

The details of the multispectral data images and the methodology to achieve LULC change detection covering the study area are shown in Fig. 4 and Table 1.

Several remotely sensed data were used in QLGs such as Landsat MSS data, Landsat 5 TM, Landsat 7 ETM + , and Landsat 8 OLI/TIRS satellite images. They were acquired on different dates in 1984, 1990, 2000, 2010, and 2018 and obtained freely from The United States Geological Survey (USGS) website (https://glovis.usgs.gov/). All Landsat images used in this study are prereferenced with WGS 84 datum. Field verification and Google Earth images have been done in geometric corrections.

There is a reverse relationship between the amount of cloud covering satellite images and the quality of the classification of images. So, we should choose a cloudless

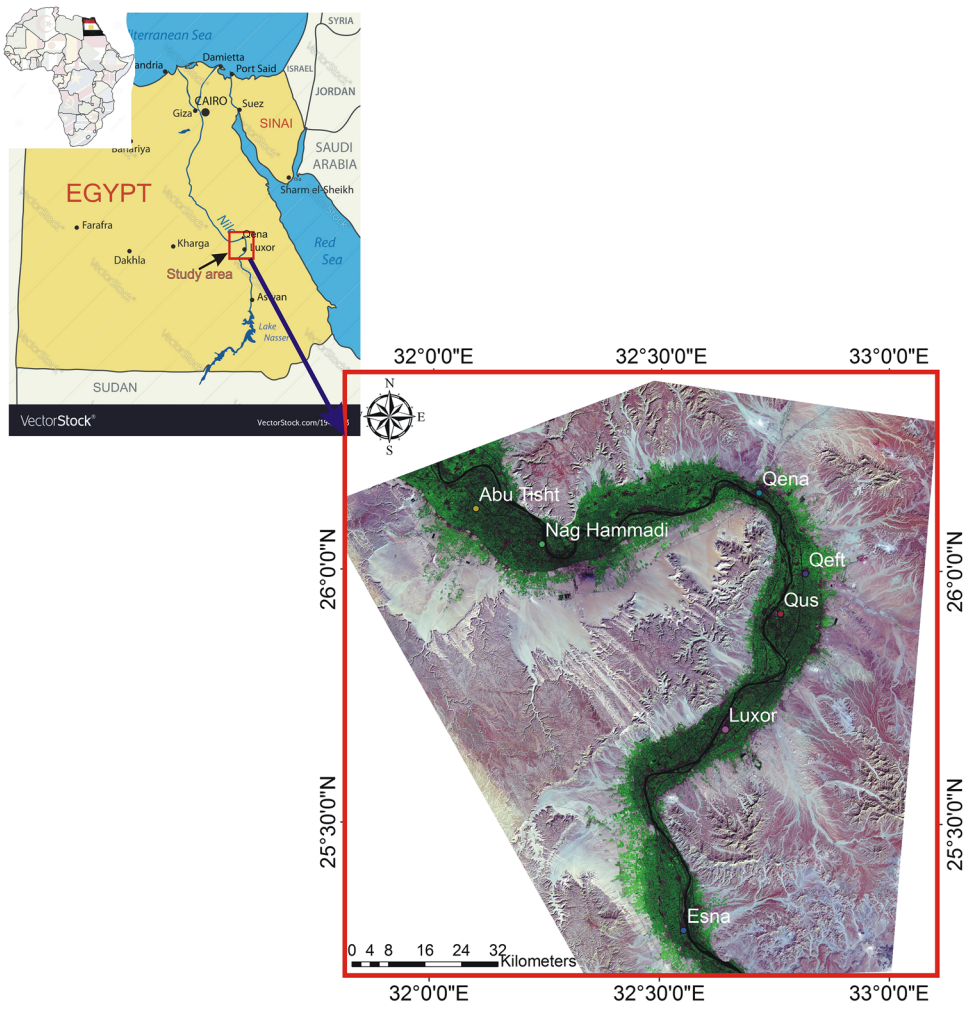

Fig. 1 Location map of Africa, Egypt and Qena-Luxor area

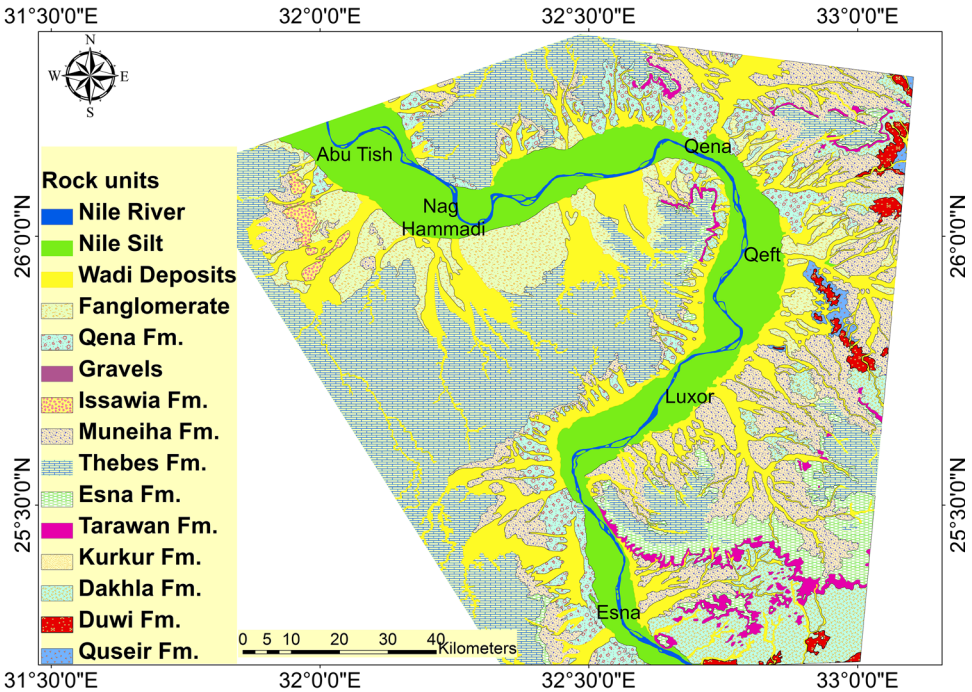

Fig. 2 Geological map of the study area (modified after CONOCO and EGPC 1987) and a composite stratigraphic column of the Nile Valley (Said 1981; Omer 1996; Issawi et al. 2009)

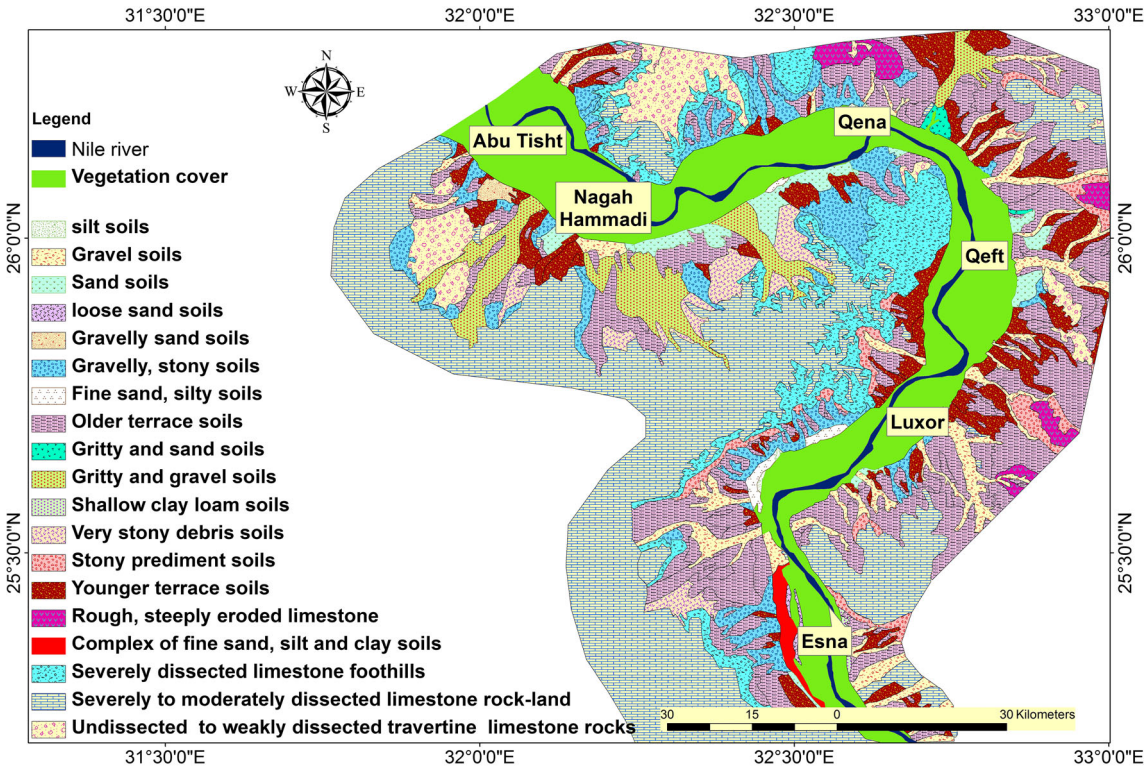

Fig. 3 Surface soils distribution map in the study area

period. For this reason, the best period is the summer season. In Egypt, the summer season starts in May and extends to August while the transitional period from summer to spring is September and October. SRTM (DEM) with 30 m also was used. These data were prepared, subset, and processed. To process the remotely sensed data, Envi 5.1, Erdas Imagine 2014, and Arc GIS 10.2 were used.

Methodology

Several methods have been used in this study; post-digital image classification and NDVI were applied. Broadly, the proposed methodology consists of several major phases. The first and important phase is the preprocessing of satellite images. The preprocessing techniques of images are a basic step and are required for fixing raw data for advanced procedures. Several steps under preprocessing techniques are utilized for the detection of LULC changes in the QLG area. These steps include layer stacking, resolution merge (pan-sharpening), radiometric and atmospheric corrections, and subsetting images. Finally, supervised classification was performed for the analysis of LULC changes, and the classifier performance is evaluated based on recognized measures from the remotely sensed data. All these stages are arranged step by step to configure and enhance the raw remotely sensed satellite data before the data improvement process is completed.

Land Use Land Cover Classifications

The spectral signature of various land cover classes in the QLG area was differentiated and recognized (Fig. 5). The results show that the proposed reclaimed desert lands have strong reflectance in all bands. The urban class has slightly moderate reflectance, but it has high reflectance in bands 5 and 6. On the other hand, water bodies have strong absorption in all bands. The agricultural land has high absorption in bands 1–4 and 6 and 7, but it has a high reflectance behavior in band 5. The agricultural land includes areas of sugar cane, wheat, corn, and some fruit crops; the sugar cane crop covers the largest agricultural area in the QLGs. Reclaimed lands are represented by the lowland fringe desert on the two Nile River banks. The LULC classes in the present study are summarized in Table 2.

Image classification is a very effective tool in explaining the process of pixel allocation in a remotely sensed image to a special land use type. Two types of image classification were applied: supervised and unsupervised classifications. In general, most authors have applied supervised classification because it is more accurate than the unsupervised one. To show LULC changes with different time

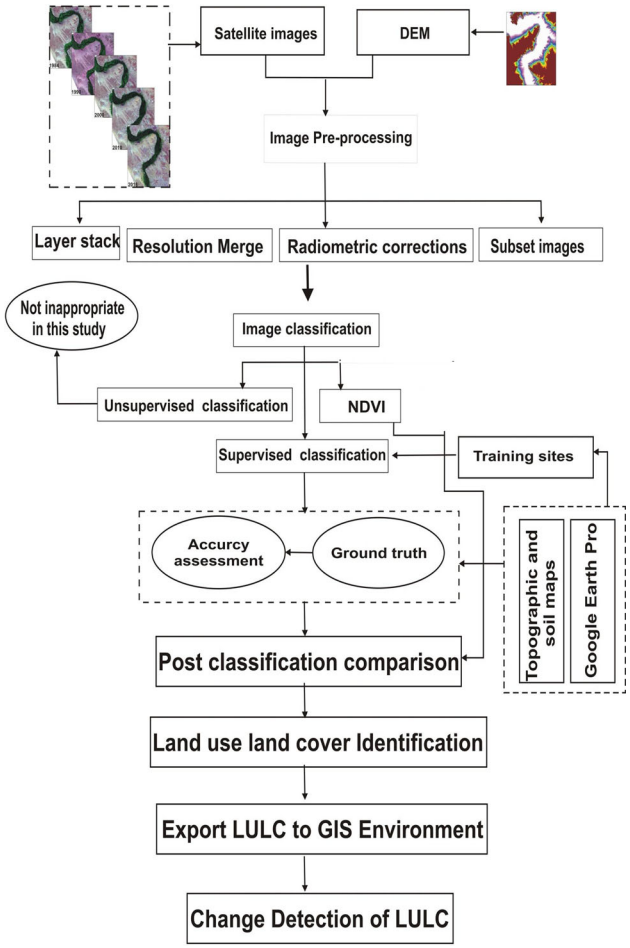

Fig. 4 Flowchart of the applied methodology framework for LULC changes detection

scales, the maximum likelihood method has been used as it is the most perfect and best type of supervised classification techniques.

Five different land use classes were got based on the number of collected signatures. About 500 area of interest (AOI) signatures were carefully captured from each image used in the present study to detect each land use class properly. Then, the ground truth points have been taken in order to confirm the results of the classification and interpretation of land cover changes.

Method to Calculate Spatial Index (NDVI)

One of the most important tools is the normalized difference vegetation index (NDVI) besides supervised classification which was applied and calculated in this study for land use change detection especially for cultivated land (Bakr et al. 2010; Khaliq et al. 2018; Tassopoulou et al. 2019). This index was calculated to show the relationship between vegetation cover and surface temperature.

Townshend and Justice (1986) used the following formula to calculate NDVI (1):

$$\mathrm{NDVI} = (\mathrm{NIR} - \mathrm{Red}) / (\mathrm{NIR} + \mathrm{Red}). \quad (1)$$

Two bands of Landsat satellite data were used to perform NDVI processing: (1) visible red band with reflectance (600–700 nm) and (2) Near-Infrared Reflectance (NIR) (750–1300 nm). The wavelength value of each band changed from one Landsat to another, based on the spectral resolution of data.

Four Landsat generations were used in this study with five time series: the Landsat TM 5 (1984) bands 3 and 4, Landsat 5 MSS (1990) bands 3 and 2, Landsat 7 ETM + (2000), Landsat 5 TM (2010) bands 3 and 4, and Landsat 8 OLI (2018) bands 4 and 5. NDVI values ranged from − 1 for nonvegetation cover to + 1 for vegetation cover.

The results obtained from NDVI ranged from − 1 to + 1, where the positive sign fits in with the higher pixel values, indicating the presence of dense vegetation cover. Pixels from other classes have a digital number equal to or less than zero, while the soil values were less than 0.5. Over the past decade, NDVI indices have been generated for dense forest areas, as well as new functionalities allowed by recent multispectral sensors (Addabbo et al. 2016).

Accuracy Assessment

Several researchers have applied the accuracy assessment method on supervised techniques to confirm the accurate relationship between actual and predicted classes employing a classification system using an error matrix (Lucas and van der Wel 1994; Stehman and Czaplewski, 1998; Van Deusen 1996; Yohanis et al. 2014). One of the most important results of accuracy assessment is related to the overall accuracy of the map, as well as each class in the classified map. Overall accuracy, in terms of percentages, can be calculated by the following equation:

$$\text{Overall accuracy} = (\text{Total number of true samples} / \text{Total number of samples}) \times 100.$$

Error matrices were applied for supervised classification concerning the true ground and classified pixel information for each LULC class. Four outputs can be derived from error matrices, where the statistics are related to the supervised classification image used in the present study: (1) the producer's accuracy, (2) the user's accuracy, (3) overall accuracy, and (4) kappa statistics.

Five categories of kappa coefficient are observed, namely, slight (0–0.20), fair (0.21–0.40), moderate

Table 1 Spectral and Spatial resolution data source of remotely sensed data

	Sensor date path/raw	sun azimuth	Land cloud cover	Sun elevation	Earth sun deviation	Bands	Wavelength (mμ)	Spatial resolution (m)
1	LT05_L1TP Thematic Mapper (TM)	123.68	0	61.9390	–	Band 1- B	0.45–0.52	30
	05/24/1984					Band 2- G	0.52–0.60	30
	175/042					Band 3- R	0.63–0.69	30
						Band 4- (NIR)	0.76–0.90	30
						Band 5- (SWIR) 1	1.55–1.75	30
						Band 6-Thermal	10.40–12.50	120*(30)
						Band 7 (SWIR) 2	2.08–2.35	30
2	LM5 Multispectral Scanner (MSS)	111.66	0	54.4213	1.0098	Band 1- G	0.5–0.6	60
	08/29/1990					Band 2-R	0.6–0.7	60
	175/042					Band 3-(NIR)	0.7–0.8	60
						Band 4-(NIR)	0.8–1.1	60
3	L7 Enhanced Thematic Mapper Plus (ETM +)	147.062	0	48.2143	0.99577	Band 1-B	0.45–0.52	30
						Band 2-G	0.52–0.60	30
	10/19/2000					Band 3-R	0.63–0.69	30
	175/042					Band 4-(NIR)	0.77–0.90	30
						Band 5 -(SWIR) 1	1.55–1.75	30
						Band 6-Thermal	10.40–12.50	60 * (30)
						Band 7 -(SWIR) 2	2.09–2.35	30
						Band 8-Panchromatic	0.52–0.90	15
4	LT05_L1TP_ Thematic Mapper (TM)	90.96	0	66.75009	1.0159	Band 1- B	0.45–0.52	30
	06/17/2010					Band 2- G	0.52–0.60	30
	175/042					Band 3- R	0.63–0.69	30
						Band 4- (NIR)	0.76–0.90	30
						Band 5- (SWIR) 1	1.55–1.75	30
						Band 6-Thermal	10.40–12.50	120*(30)
						Band 7 (SWIR) 2	2.08–2.35	30
5	LC08_ LC08_L1TP Landsat 8 Operational Land Imager (OLI) and (TIRS)	122.94	0	68.9402	1.0148	Band 1-Ultra Blue (coastal/aerosol)	0.435-0.451	30
						Band 2-B	0.452–0.512	30
	06/07/2018					Band 3-G	0.533–0.590	30
	175/042					Band 4-R	0.636–0.673	30
						Band 5-(NIR)	0.851–0.879	30
						Band 6 -(SWIR) 1	1.566–1.651	30
						Band 7 -(SWIR) 2	2.107–2.294	30
						Band 8-Panchromatic	0.503–0.676	15
						Band 9-Cirrus	1.363–1.384	30
						Band 10-Thermal Infrared (TIRS) 1	10.60–11.19	100 * (30)
						Band 11-Thermal Infrared (TIRS) 2	11.50–12.51	100 * (30)

(0.41–0.60), substantial (0.61–0.80), and almost perfect agreement (0.81–1).

The accuracy assessment results for this study were calculated for land use maps of series Landsat data during 1984, 1990, 2000, 2010, and 2018. The overall accuracy in 1984 and 1990 was found to be 91.2% and 92.5%, respectively, while the kappa coefficient was 0.88 and 0.90, respectively (see Tables 3 and 4). In 2000 and 2010, the

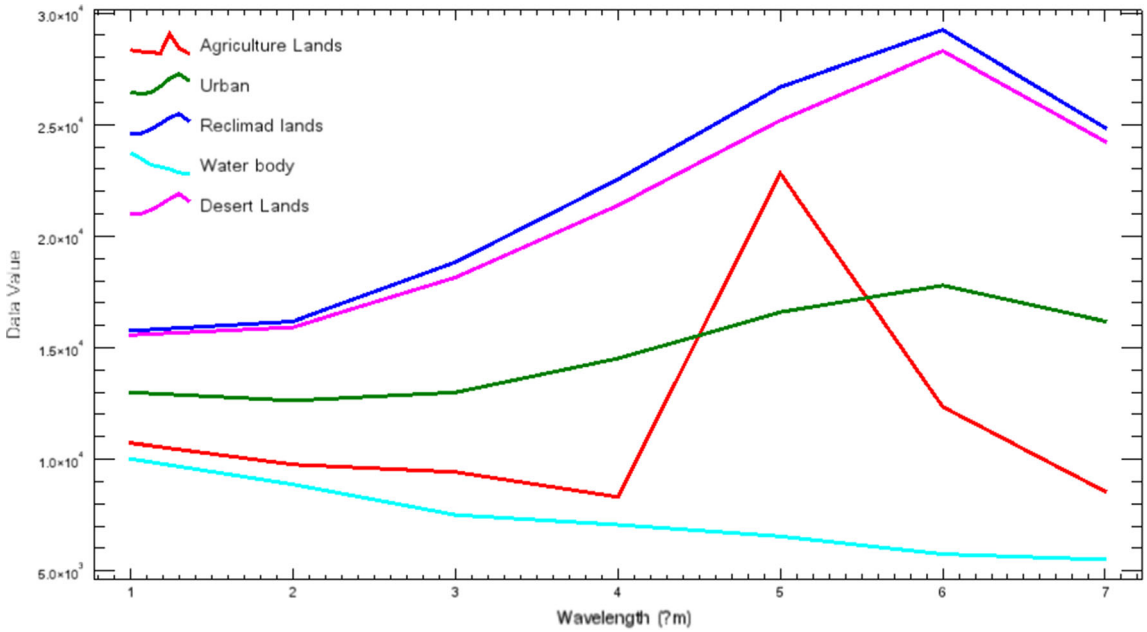

Fig. 5 Spectral signatures available land cover in the study area

Table 2 Land use/cover classification scheme

	Land cover classes	Description
1	Agriculture lands	Cultivated lands, trees areas sparsely vegetated areas, periodic and temporary irrigation agriculture, crops such as sugar cane, wheat, corns, and other winter crops
2	Urban	Areas with built-up (residential, commercial, industrial, transportation, airports, roads railways, and facilities)
3	Water body	Water areas (River Nile, canals and drains)
4	Low lands areas	Reclaimed areas, uncultivated agricultural lands, desert fringes
5	Desert lands	Surface areas that are removed to expose deposits such as limestone plateau in east and west limits of the studied area

land use classified maps of Landsat 7 ETM + and Landsat 5 TM show that the overall accuracy is 91% and 87.1%, with the kappa coefficient being 0.88 and 0.83, respectively (see Tables 5 and 6). In 2018, the land use maps of LC08 Landsat 8 (OLI) show that the overall accuracy is 92.5%, with the kappa coefficient being 0.90 (see Table 7). The

Table 3 Accuracy assessments of land use land cover classes of Landsat-5 TM data classified in1984 in the study area

1984	Agriculture lands	Urban	Water body	Reclamation lands	Desert lands	Total true samples	Total samples	User's accuracy
Agriculture lands	151	0	12	3	0	–	166	90.96
Urban	5	98	4	0	0		107	91.58
Water body	1	0	75	4	0		80	93.75
Reclamation lands	0	5	0	139	33		177	78.53
Desert lands	1	1	0	1	267		270	98.89
Total true samples						730		
Total samples	158	104	91	147	300	800		
Producer's accuracy	95.56	94.23	82.41	94.55	89	Overall accuracy 91.2%		
						Kappa coefficient 0.88		

Table 4 Accuracy assessments of land use land cover classes of Landsat-5 MSS data classified in1990 in the study area

1990	Agriculture lands	Urban	Water body	Reclamation lands	Desert lands	Total true samples	Total samples	User's accuracy
Agriculture lands	188	0	22	0	0		210	89.52
Urban	5	95	4	0	0		104	91.34
Water body	1	0	80	0	0		81	98.76
Reclamation lands	0	4	0	90	22		116	77.58
Desert lands	1	0	0	1	287		289	99.30
Total true samples						740		
Total sample	195	99	106	91	309	800		
Producer's accuracy	96.41	95.95	75.47	98.90	92.88	Overall accuracy 92.5%		
						Kappa coefficient 0.90		

present author observed that the producer's and user's accuracies were found to be above 75% for all land use classes, except water body and urban areas. The producer's accuracy of water bodies was 71.63% and 53.19% in 2000 and 2010, respectively, while the user's accuracy of the urban class was 68.92% in 2010. This low percentage of water bodies and urban areas is due to the confusion of having mixed pixels between these two classes and agricultural lands and desert land classes, respectively. In other words, this is due to the diverse materials found on different surfaces, although the enhancement of the remotely sensed data was undertaken before applying the supervised classification technique.

Results and Discussions

In this paper, the final classified thematic maps were created by maximum likelihood supervised classification and NDVI methods in order to detect quantitative LULC change detection in the present area during the period from 1984 to 2018.

Post-supervised classification is used to monitor the change of land cover (Lu et al. 2004). It produces a complete matrix of change direction by Landsat data that are classified independently (Alphan et al. 2009; Solaimani et al. 2010; Yang and Wen 2011).

Post-Supervised Classification of LULC

The change detection of LULC classes obtained by the classification of mutilated optical satellite imageries of the QLG study was calculated. The imageries of the satellite over 34 years (1984–2018) of Qena-Luxor Governorates were analyzed and displayed in five final classified thematic maps.

The outcomes of the supervised classification reported that general agricultural and urban classes increased during the time series 1984–2018. In addition, the reclaimed lands increased from 1984 to 2000, then decreased from 2000 to 2010, and noticeably increased in the period from 2010 to

Table 5 Accuracy assessments of land use land cover classes of Landsat-5 TM data classified in 2000 in the study area

2000	Agriculture lands	Urban	Water body	Reclamation lands	Desert lands	Total true samples	Total samples	User's accuracy
Agriculture lands	128	17	13	0	1		159	80.5
Urban	2	140	27	0	0		169	82.84
Water body	0	0	101	0	0		101	100
Reclamation lands	0	1	0	96	4		101	95.05
Desert lands	1	2	0	4	263		270	97.40
Total true samples						728		
Total sample	131	160	141	100	268	800		
Producer's accuracy	97.71	87.5	71.63	96	98.13	Overall accuracy 91%		
						Kappa coefficient 0.88		

Table 6 Accuracy assessments of land use land cover classes of Landsat-7 ETM + data classified in 2010 in the study area

2010	Agriculture lands	Urban	Water body	Reclamation lands	Desert lands	Total true samples	Total samples	User's accuracy
Agriculture lands	127	5	1	1	0		134	94.77
Urban	4	153	64	1	0		222	68.92
Water body	0	0	75	0	0		75	100
Reclamation lands	0	0	1	91	17		109	83.48
Desert lands	1	2	0	6	251		260	96.53
Total true samples						697		
Total sample	132	160	141	99	268	800		
Producer's accuracy	96.21	95.62	53.19	92	93.65	Overall accuracy 87.1%		
						Kappa coefficient 0.83		

Table 7 Accuracy assessments of land use land cover classes of Landsat-8 OLI data classified in2018 in the study area

2018	Agriculture lands	Urban	Water body	Reclamation lands	Desert lands	Total true samples	Total samples	User's accuracy
Agriculture lands	146	6	1	0	0		153	95.42
Urban	2	134	25	3	0		164	81.70
Water body	3	0	114	0	0		117	97.43
Reclamation lands	1	1	2	108	10		122	88.52
Desert lands	0	0	0	6	238		244	97.54
Total true samples						740		
Total sample	152	141	142	117	248	800		
Producer's accuracy	96.05	95.035	80.28	92.30	95.96	Overall accuracy 92.5%		
						Kappa coefficient 0.90		

2018. The desert lands were decreased with the increase of other classes recorded in the study area during the selected time series (1984–2018). Each land cover class has been calculated in a square kilometer, and the percentage during the selected time is listed in Table 8.

The LULC Maps

The five classes (i.e., agricultural lands, water bodies, reclaimed lands, desert lands, and built-up areas) were detected and stored in a GIS environment. The supervised classification of land use maps in 1984 and 2000 was created using Landsat 5 TM satellite imagery, as shown in Fig. 6a, b), that in 1990 was produced by Landsat 5 MSS (Fig. 6c), and that in 2010 was generated from Landsat 7 ETM + satellite imagery (Fig. 6d). In addition, the land use map was created based on Landsat 8 (OLI) images from 2018 (Fig. 6e). The LULC maps of the QLG area between 1985 and 2018 were measured in km^2, presented and tabulated in Fig. 6f and Table 8.

The agricultural land in the QLG area has been developed over the previous thirty-four years. They have dramatically changed from 1984 to 2018; it increased from 1238.7 to 1346.6 km^2 from 1984 to 1990, respectively. It increased to 1530.3 km^2, 1658.19 km^2, and 1707.04 km^2 in 2000, 2010, and 2018, respectively.

Another best method used to detect vegetation lands (agricultural class in the present study) is the NDVI. This method is unique because it easily identifies and detects the agricultural land class from other classes. The results of this method nearly fit in with the supervised classification results of the agricultural land class during all selected years.

The desert lands, representing the highlands surrounding the lowlands of the Wadi El Nile area, covered 6635.4 km^2 (52.1%) in 1984. This class slightly decreased to 6477.4 km^2 (50.87%) in 1990 and 6171.74 km^2 (48.47%), 6150.63 km^2 (48.3%), and 6003.5 km^2 (47.15%) in 2000, 2010, and 2018, respectively (Table 8).

New proposed reclaimed lands cover about 4379.7 km^2 (34.39%) in 1984, increased in 1990 and 2000 to 4419.6

Table 8 Comparison of areas of change of the five LULC classes based on supervised classification between 1984 and 2018

	1984		1990		2000		2010		2018	
	Area (Km^2)	%	Area (Km^2)	%	Area (Km^2)	%	Area (Km^2)	%	Area (Km^2)	%
Agriculture lands	1238.7	9.8	1346.6	10.6	1530.3	12.018	1658.19	13.023	1707.04	13.40
Proposed reclamation lands	4379.7	34.4	4419.6	34.7	4521.05	35.507	4373.51	34.35	4442	34.89
Desert lands	6635.4	52.2	6477.4	50.9	6171.74	48.48	6150.63	48.31	6003.5	47.15
Urban	345.2	2.7	354.1	2.8	375.048	2.95	415.42	3.26	445.28	3.5
Water body	133.9	1.055	134.4	1.056	134.5	1.0565	134.55	1.057	135	1.06
Total	12,732	–	12,732	–	12,732	–	12,732	–	12,732	–
	NDVI									
	1984		1990		2000		2010		2018	
Vegetation cover	1204	9.45	1323	10.39	1518	11.92	1631	12.81	1688	13.25

km^2 (34.71%) and 4521.05 km^2 (35.50%), respectively, but then in 2010 decreased to 4373.51 km^2 (34.34%). On the other hand, the reclaimed land increased to about 4442 km^2 (34.88%) in 2018 (see Table 8).

Urban areas increased rapidly between 1984 and 2018, including housing, roads, industrial areas, and other human activities. Population growth and the wider development of roadways related to industry and new urban communities have led to a considerable increase in urban areas, from about 345.2 km^2 (2.71%) in 1984 to approximately 354.1 km^2 (2.78%) in 1990, 375.048 km^2 (2.94%) in 2000, and 415.42 km^2 (3.26) in 2010. In addition, the urban areas increased clearly during the period from 2010 to 2018, as citizens fled from the narrow Nile Valley to the low-lying desert fringe (proposed reclaimed lands) areas overgrown for the limestone plateau, up to 445.28 km^2 (3.5%) (see Table 8).

Water bodies in 1984 covered an area of about 133.9 km^2 with 1.051%, slowly increasing to approximately 134.4 km^2 (i.e., 1.055% of the total study area) in 1990, increasing in 2000, 2010, and 2018 to about 134.5 km^2 (1.056%), 134.53 km^2 (1.057%), and 135 km^2 (1.06%), respectively (see Tables 3 and 4). This class has remained relatively unchanged in the present study due to the lack of new channels and banks, in addition to the low water level of the Nile River due to the construction of some dams in some upstream countries.

NDVI Processing

The NDVI outcome distribution between 1984 and 2018 (Figs. 7a–e) revealed that the highest values were recorded in 2000 (+ 0.992), 1984 (+ 0.71), 2010 (0.691), and 1990 (+ 0.666), and the lowest values (+ 0.6) were recorded in 2018. On the other hand, the area was characterized by high NDVI values ranging from + 0.6 to + 0.99. These NDVI values and maps were used to detect the changes in vegetation over the study period.

The area was found to have moderate NDVI values, corresponding to a mixture of bare soils and areas covered by photosynthetic active vegetation (Mondal et al. 2017; Castaldi et al. 2019). Vegetation index differencing is also widely used to identify changes in LULC, in particular, those related to shifting cultivated areas (Rao et al. 2018). Remotely sensed data are vital to the activity of highlighting vegetation cover characteristics using the NDVI method for assessing and managing natural resources. The major activities influencing these changes in vegetation were found to be related to agriculture. The results indicated that vegetation cover in the QLG area from 1984 to 2018 nearly fits in with that extracted by the maximum likelihood classification over the same time series of the remotely sensed data (see Fig. 7f and Table 8).

Change Detection

Changes in the five selected LULC classes were determined and detected for the MLC classified maps to calculate the changes in the QLG study area in the time series 1984–2000, 2000–2010, and 2010–2018.

The QLG area covers about 12,732 km^2 and is classified into five classes as shown in Table 9. The desert lands represent almost half of the study area. The class of agricultural lands covers about 10% of the study area. It is concentrated along the two banks of the Nile River.

This study established that the current area experienced a number of dramatic changes between 1984 and 2018, particularly in relation to agricultural lands, urban areas, water bodies, reclaimed lands, and desert areas.

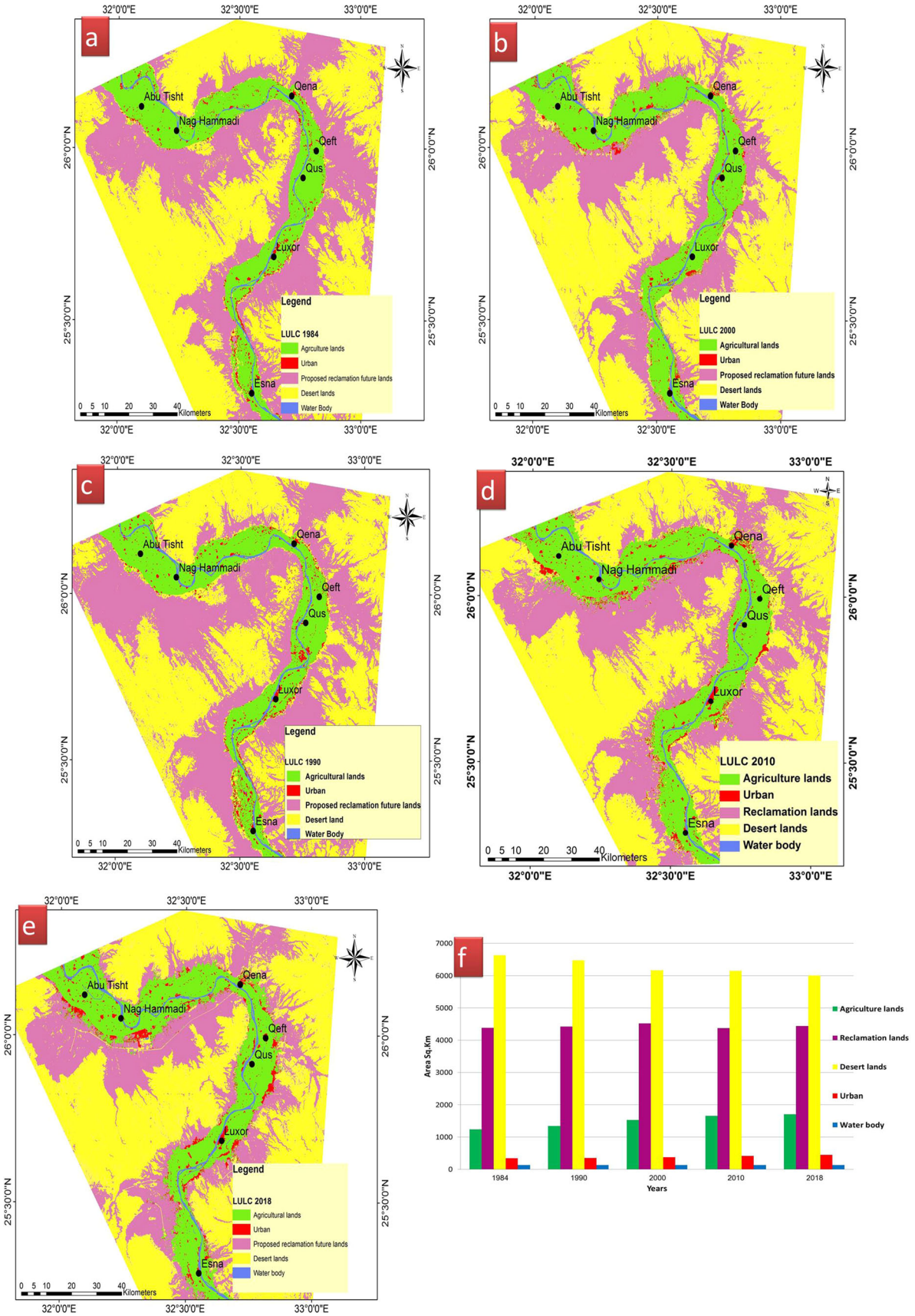
a
b
c
d
e
f
32°0'0"E
32°30'0"E
33°0'0"E
26°0'0"N
25°30'0"N
Abu Tisht
Nag Hammadi
Qena
Qeft
Qus
Luxor
Esna
Legend
LULC 1984
Agriculture lands
Urban
Proposed reclamation future lands
Desert lands
Water Body
LULC 2000
Agricultural lands
Urban
Proposed reclamation future lands
Desert lands
Water Body
LULC 1990
Agricultural lands
Urban
Proposed reclamation future lands
Desert land
Water Body
LULC 2010
Agriculture lands
Urban
Reclamation lands
Desert lands
Water body
LULC 2018
Agricultural lands
Urban
Proposed reclamation future lands
Desert lands
Water body
0 5 10 20 30 40 Kilometers
Area Sq.Km
Years
1984
1990
2000
2010
2018
Agriculture lands
Reclamation lands
Desert lands
Urban
Water body

◀**Fig. 6** LULC maps resulting by supervised classification methods (**a**-1984, **b**-2000 **c**-1990, **d**-2010 and **e**-2018); **f**- Area of LULC classes as square kilometer of all classes of the landscape over 1984, 1990, 2000, 2010, and 2018

Finally, during 34 years, in the QLG study area, the outcomes of the land use land cover change detection indicate that all classes herein were subjected to change. The increased and decreased changes over the five selected time series (1984, 1990, 2000, 2010, and 2018) in each class in the study area are illustrated in Fig. 8 and summarized in Table 9.

Based on the results of change detection, the present author reported that all classes were increased within all periods except desert lands that were decreased during the same period and the reclaimed lands that were decreased in the period from 2000 to 2010.

In 1984, the urban area covered 345.2 km^2 (2.71%) (representing cities, villages, factories, and asphaltic roads along the Nile River and Wadi El Nile lowlands), but it increased to approximately 354.1 km^2 in 1990 with an increase of about 8.9 km^2 and to 375.048 km^2 in 2000 with an average increase of about 20.948 km^2. Moreover, there is also an increase of about 40.37 km^2 in the period between 2000 and 2010. During 2010–2018, the urban area increased by about 29.86 km^2 (see Fig. 9a–d).

The agricultural area initially increased from 1238.7 km^2 (9.72%) in 1984–1530.3 km^2 (12.018%) in 2000 and then increased to 1707.04 km^2 (13.40%) in 2018 (see Fig. 9a–d).

The results indicate that the proposed reclaimed areas expanded in the study area in the assigned time series within desert fringes and related to lowland areas. The study showed that the area of reclaimed lands increased significantly, i.e., from 4379.7 km^2 (34.64% of the total area of the study area) in 1984 to 4521.05 km^2 (35.5%) in 2000. During the period from 2000 to 2010 and during the revolution of January 25, 2011, the reclaimed lands decreased from 4521.05 km^2 in 2000 to 4373.51 km^2 in 2010, with surface change detection of about -147.54 km^2. After that stage, this class again increased to 4442 km^2 in 2018 with an increase of about 68.49 km^2 (see Fig. 9a–d and Table 9).

The reclaimed lands have changed from 4379.7 km^2 to 4419.6 km^2 during the period from 1984 to 1990 with an approximate increase of 39 km^2 (0.315%). The area that has a change of LULC increased by about 101.45 km^2 (0.8%) from 1990 to 2000. During 2000–2010, the reclaimed land class decreased around − 147.54 (1.4%). Then, it started to increase again in the period from 2010 to 2018 (around 68.49 km^2, 0.53%).

The desert lands decreased from 6635.4 km^2 (52.11%) in 1984 to 6150.63 km^2 (48.30%) in 2010 and then to 6003.5 km^2 (47.14%) in 2018 (see Fig. 9a–d). The limestone plateau and wadis desert are the reasons behind the decrease in this class leading to the prevention of the use of agricultural, economic, and urban projects. This class is considered the largest class in the study area.

Consequentially, we can report that the water body class during the studied period was slightly constant with light increase. It increased about 0.52 km^2 (0.004%) from 1984 to 1990. Moreover, 0.17 km^2 (0.000741%), 0.12 km^2 (0.00011%), and about 0.50 km^2 (0.00388%) were recorded on classified Landsat images in the periods 1990–2000, 2000–2010, and 2010–2018, respectively. Generally, it increased from 1.05 to 1.06% (Table 9).

The built-up class has been changed with an increase of 8.9 km^2 from 1984 to 1990 and about 20.948 km^2, 40.372 km^2, and 29.86 km^2 from 1990 to 2000, 2000 to 2010, and 2010 to 2018, respectively (Figs. 9a–d). According to these results, we note that urbanization increased significantly in the period from 2000 to 2010 compared to the other periods selected in this study.

Conclusions

The Qena-Luxor Governorates have been selected as a case study to report that remotely sensed data in the GIS environment are essential for the detection of land use land cover changes. The detection of the land use land cover changes by the maximum likelihood supervised classification and NDVI is a valuable resource for decision-makers to plan future sustainable development projects. Five land cover classes were detected in the current study based on the image classification, namely, agricultural lands, urban areas, water bodies, reclaimed lands, and desert lands.

The outcomes display that water bodies representing the Nile River and irrigation drains and channels slightly increased from 133.9 to 135 km^2 in the period from 1984 to 2018. The urban class increased from 345.2 to 445.28 km^2 (2.7–3.5%). Furthermore, the desert lands lost about 631.9 km^2 (4.94%) from the total area of the QLGs. Meanwhile, the reclaimed class has shown a considerable increase of 141.35 km^2 (1.11%) between 1984 and 2000. But, this class decreased after 2000, as a result of the agricultural and urban expansion in addition to the shortage of land reclamation. Then, it increased after 2010. The study indicated that the spread of agricultural lands increased between 1984 and 2018. Change detection is made possible by these technologies in less time, at low cost, and with better accuracy. The accuracy assessment technique was applied to all selected remotely sensed images. It

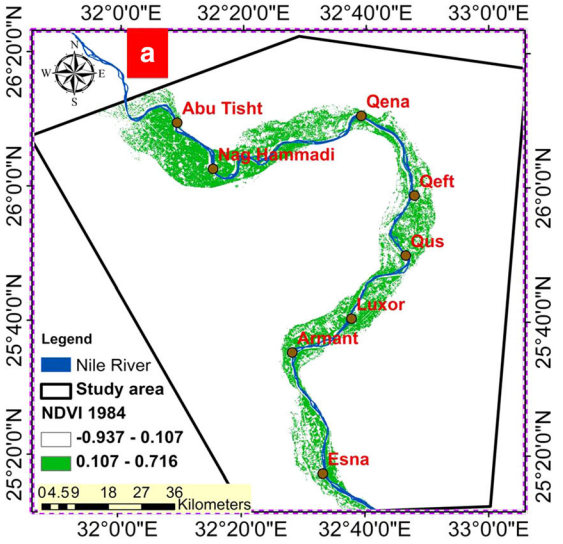
a
Abu Tisht
Qena
Nag Hammadi
Qeft
Qus
Luxor
Armant
Esna
Legend
Nile River
Study area
NDVI 1984
-0.937 - 0.107
0.107 - 0.716
04.59 18 27 36
Kilometers
32°0'0"E
32°20'0"E
32°40'0"E
33°0'0"E
26°20'0"N
26°0'0"N
25°40'0"N
25°20'0"N

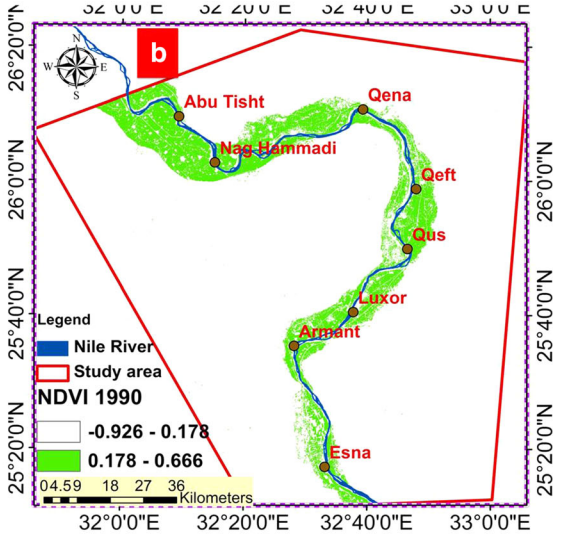
b
Abu Tisht
Qena
Nag Hammadi
Qeft
Qus
Luxor
Armant
Esna
Legend
Nile River
Study area
NDVI 1990
-0.926 - 0.178
0.178 - 0.666
04.59 18 27 36
Kilometers
32°0'0"E
32°20'0"E
32°40'0"E
33°0'0"E
26°20'0"N
26°0'0"N
25°40'0"N
25°20'0"N

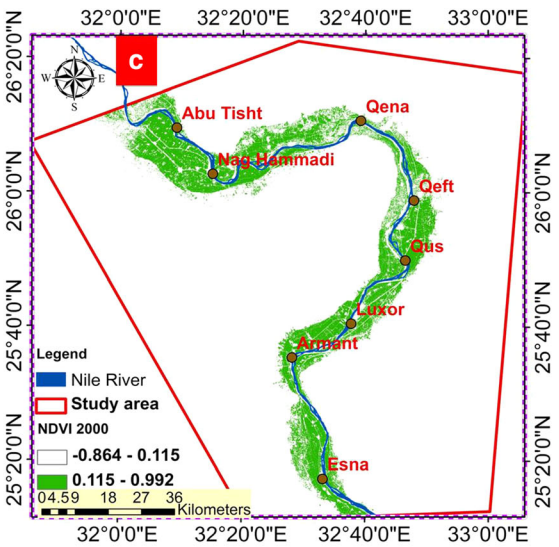
c
Abu Tisht
Qena
Nag Hammadi
Qeft
Qus
Luxor
Armant
Esna
Legend
Nile River
Study area
NDVI 2000
-0.864 - 0.115
0.115 - 0.992
04.59 18 27 36
Kilometers
32°0'0"E
32°20'0"E
32°40'0"E
33°0'0"E
26°20'0"N
26°0'0"N
25°40'0"N
25°20'0"N

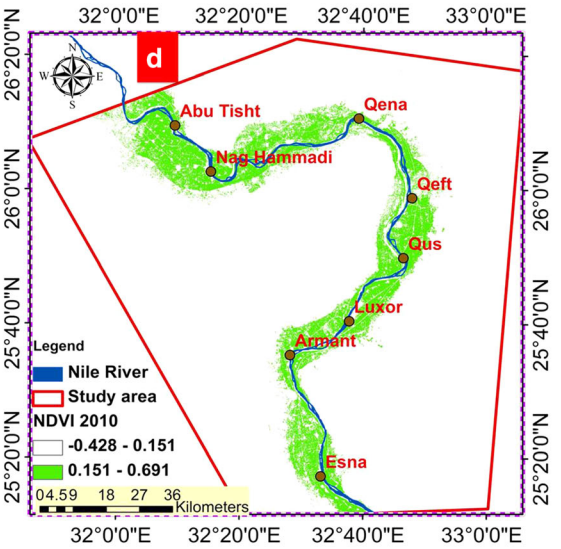
d
Abu Tisht
Qena
Nag Hammadi
Qeft
Qus
Luxor
Armant
Esna
Legend
Nile River
Study area
NDVI 2010
-0.428 - 0.151
0.151 - 0.691
04.59 18 27 36
Kilometers
32°0'0"E
32°20'0"E
32°40'0"E
33°0'0"E
26°20'0"N
26°0'0"N
25°40'0"N
25°20'0"N

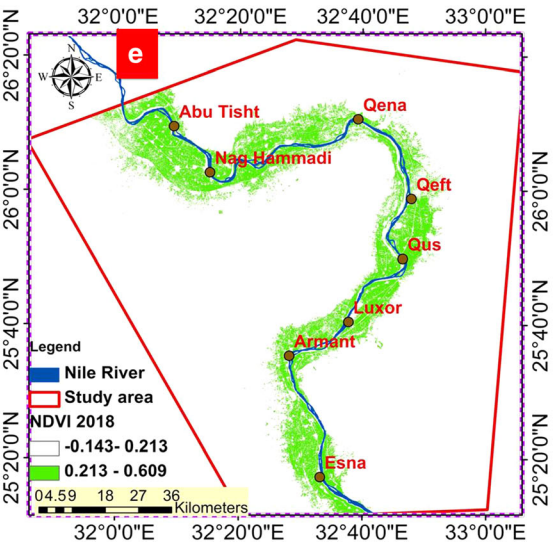
e
Abu Tisht
Qena
Nag Hammadi
Qeft
Qus
Luxor
Armant
Esna
Legend
Nile River
Study area
NDVI 2018
-0.143- 0.213
0.213 - 0.609
04.59 18 27 36
Kilometers
32°0'0"E
32°20'0"E
32°40'0"E
33°0'0"E
26°20'0"N
26°0'0"N
25°40'0"N
25°20'0"N

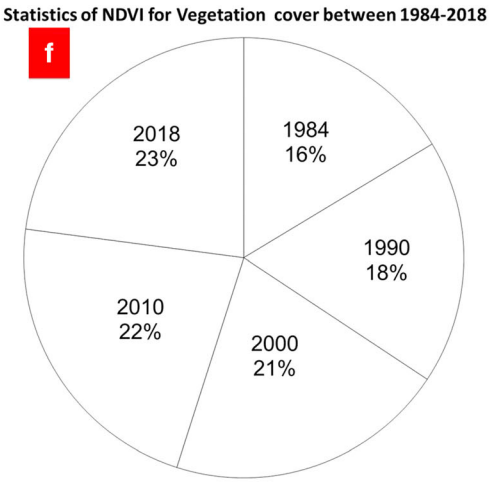
Statistics of NDVI for Vegetation cover between 1984-2018
f
2018
23%
1984
16%
1990
18%
2010
22%
2000
21%

◀**Fig. 7** Normalized difference vegetation index (NDVI) thematic maps of Landsat images (**a**-1984, **b**-1990 **c**-2000, **d**-2010 and **e**-2018) of the (QLG) area

Table 9 Area under change of Land Use/Land Cover Categories during 1984–2018 based on supervised classification in Qena-Luxor Governorate (QLG) area

	1984–1990		1990–2000		2000–2010		2010–2018	
	Different (Km^2)	%	Different (Km^2)	%	Different (Km^2)	%	Different (Km^2)	%
Agriculture lands	107.9	0.848076	183.7	1.442302	127.89	1.004813	48.85	0.3830
Reclamation lands	39.9	0.315542	101.45	0.795305	− 147.54	− 1.15773	68.49	0.5363
Desert lands	− 158	− 1.23768	− 305.66	− 2.40275	− 21.11	− 0.16436	− 147.13	− 1.1576
Urban	8.9	0.070072	20.948	0.164405	40.372	0.317172	29.86	0.2343
Water body	0.52	0.004	0.17	0.000741	0.12	0.00011	0.5	0.00388

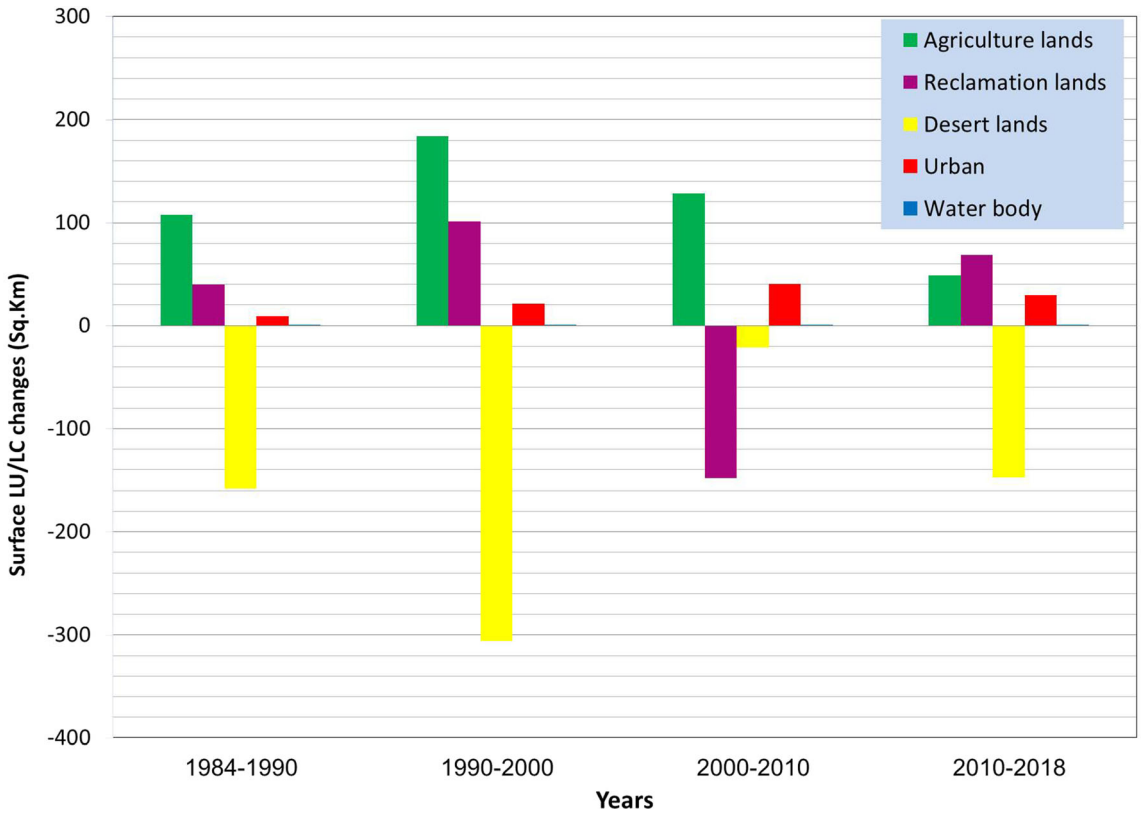

Fig. 8 The spatial distribution of LULC changes between 1984 and 2018 in the study area

confirmed that the supervised classification method is a very effective tool in detecting LULC changes in a time series. The present author recommends that the lowland areas on the two banks of the Nile River in the QLGs need more attention for the reclamation and other activities from the Egyptian government.

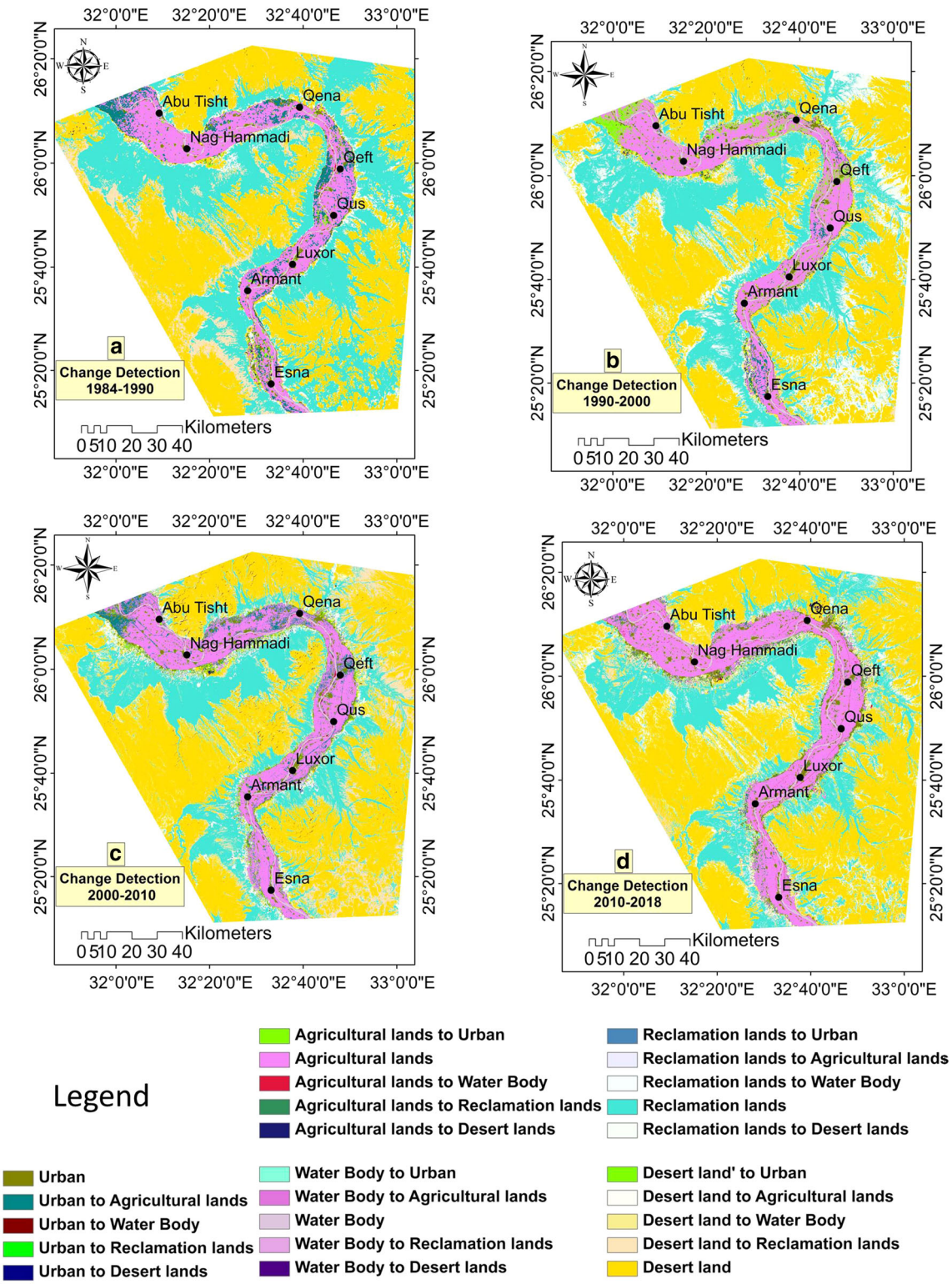

Fig. 9 The spatial distribution of land use/land cover (LULC) changes from one class to another between **a**-1984–1990, **b**-1990–2000, **c**-2000–2010 and **d**-2010, 2018 in the study area

Compliance with Ethical Standards

Conflict of interest The authors declare that they have no conflict of interest.

References

Abdalla, F., & Moubark, K. (2018). Assessment of well performance criteria and aquifer characteristics using step-drawdown tests and hydrogeochemical data, west of Qena area, Egypt. *Journal of African Earth Sciences, 138*, 336–347.

Addabbo, P., Focareta, M., Marcuccio, S., Votto, C., & Ullo, L. S. (2016). Contribution of Sentinel-2 data for applications in vegetation monitoring. *ACTA IMEKO, 5*(2), 44. https://doi.org/10.21014/acta_imeko.v5i2.352.

Abd El-kawy, O. R., Red, J. K., Ismail, H. A., & Suliman, A. S. (2011). Land use and land cover change detection in the western Nile delta of Egypt using remote sensing data. *Applied Geography, 31*(2), 483–494.

Allama, M., Bakrb, N., & Elbablya, W. (2019). Multi-temporal assessment of land use/land cover change in arid region based on landsat satellite imagery: Case study in Fayoum Region Egypt. *Remote Sensing Applications: Society and Environment., 14*, 8–19.

Alphan, H., Doygun, H., & Unlukaplan, I. Y. (2009). Post classification comparison of land cover using multitemporal Landsat and ASTER imagery: The case of Kahramanmaraş, Turkey. *Environmental Monitoring and Assessment, 151*, 327–336.

Amna, B., Rabia, S., Sheikh, S. A., & Neelam, A. (2015). Land use change mapping and analysis using Remote Sensing and GIS: a case study of Simly watershed, Islamabad, Pakistan. *The Egyptian Journal of Remote Sensing and Space Sciences, 18*, 251–259.

Bakr, N., Weindorf, D. C., Bahnassy, M., Marei, S. M., & El-Badawi, M. M. (2010). Monitoring land cover changes in a newly reclaimed area of Egypt using multitemporal Landsat data. *Applied Geography, 30*, 592–605.

Castaldi, F., Chabrillat, S., & van, Wesemael, B., (2019). Sampling Strategies for Soil Property Mapping Using Multispectral Sentinel-2 and Hyperspectral EnMAP Satellite Data. *Remote Sensing, 11*, 309.

Chen, J., Ban, Y., & Li, S. (2014). Open access to earth land-cover map. *Nature, 514*, 434. https://doi.org/10.1038/514434c.

Close, O., Benjamin, B., Petit, S., Fripiat, X., Hallot, E. (2018). Use of sentinel-2 and LUCAS database for the inventory of land use, land use change, and forestry in Wallonia.

Conoco, (1987). Geological Map of Egypt, Scale 1:500,000, Sheet NG36NE Quseir, NG36NW Asyut, NG36SE Gebel Hamata, and NG36SW Luxor, Egypt; The Egyptian General Petroleum Corporation: Cairo, Egypt.

Dash, C. J., Adhikary, P. P., Madhu, M., Mukhopadhyay, S. K., Singh, S. K., & Mishra, P. K. (2018). Assessment of spatial changes in forest cover and deforestation rate in Eastern Ghats Highlands of Odisha, India. *Journal of Environmental Biology, 39*(2), 196–203.

Durga, R. K. H. V., Singh, A. K., & Roy, P. S. (2009). Study of morphology and suspended sediment of Bhopal Upper Lake using spatial simulation technique and remote sensing data. *Journal of the Indian Society of Remote Sensing, 37*, 433–441.

Duraisamy, V., Bendapudi, R., & Jadhav, A. (2018). Identifying hotspots in land use land cover change and the drivers in a semi-arid region of India. *Environmental Monitoring and Assessment, 190*, 535. https://doi.org/10.1007/s10661-018-6919-5.

Faris, M., Allam A, Marzuk, A.M. (1985). Biostratigraphy of the Late Cretaceous-Early Tertiary rocks in the Nile Valley (Qena region), Egypt. Annals Geological Survival of Egypt, XV, 287–300.

FAO, (Cartographer). Reconnaissance soil map of the Nag Hammadi-Abu Tig area, Egypt. Scale 1:200,000. 1962; ESDAC. Retrived 19 May 2020, from, https://esdac.jrc.ec.europa.eu.

FAO, (Cartographer). Reconnaissance soil map of the Isna-Nag Hammadi area, Egypt. Scale 1:200,000. 1961. ESDAC. Retrived 19 May 2020, from, https://esdac.jrc.ec.europa.eu.

Gaber, A., Mohamed, A. K., El Galladi, A., Abdelkareem, M., Beshr, A. M., & Koch, M. (2020). Mapping the groundwater potentiality of West Qena Area, Egypt, using integrated remote sensing and hydro-geophysical techniques. *Remote Sensing., 12*, 1559.

Halmy, M. W. A., Gessler, P. E., Hicke, J. A., & Salem, B. B. (2015). Land use/land cover change detection and prediction in the north-western coastal desert of Egypt using Markov-CA. *Applied Geography, 63*, 101–112.

Hansen, M. C., & Loveland, T. R. (2012). A review of large area monitoring of land cover change using Landsat data. *Remote Sensing Environment, 122*, 66–74.

https://worldpopulationreview.com/.

https://gpm.nasa.gov/trmm/.

https://glovis.usgs.gov/.

Iqbal, M. F., & Khan, I. F. (2014). Spatiotemporal land use land cover change analysis and erosion risk mapping of Azad Jammu and Kashmir, Pakistan. *The Egyptian Journal of Remote Sensing and Space Sciences, 17*, 209–229.

Issawi, B., Francis, M. H., Youssef, E. S. A. A., & Osman, R. A. (2009). *The phanerozoic geology of Egypt: A Geodynamic approach* (Vol. 2). Egyptian Mineral Resources Authority (EMRA): Cairo, Egypt.

Joshi, P. K., Rashid, H., & Roy, P. S. (2002). Landscape dynamics in Hokersar wetland, Jammu and Kashmir—an application of geospatial approach. *Journal of the Indian Society of Remote Sensing, 30*(1), 1–5.

Kamel, M., & Abu El Ella, E. M. (2016). Integration of RS and GIS to Manage the sustainable Development in the Nile Valley desert fringes of Assiut-Sohag Governorates, Upper Egypt. *Journal of Indian Society of Remote Sensing, 44*(5), 759–774. https://doi.org/10.1007/s12524-015-0529-2.

Kanta kumar, L.N., Neelamsetti, P., (2015). Multi-temporal land use classifcation using hybrid approach. *The Egyptian Journal of Remote Sensing and Space Sciences, 18*, 289–295.

Khaliq, A. M. A., Musci M. Ch.(2018).Understanding effects of atmospheric variables on spectral vegetation indices derived from satellite based time series of multispectral image.IEEE Applied Imagery Pattern Recognition Workshop (AIPR), IEEE, Washington, DC, USA (2018), https://doi.org/10.1109/aipr.2018.8707430

Lambin, E. F. (1997). Modeling and Monitoring Land-Cover Change Processes in Tropical Regions. *Progress in Physical Geography, 21*, 375–393. https://doi.org/10.1177/030913339702100303.

Lambin, E. F., Turner, B. L., Geist, H. J., Agbola, S. B., Angelsen, A., Bruce, J. W., et al. (2001). The causes of land-use and land-cover change: Moving beyond the myths. *Global Environmental Changes, 11*, 261–269.

Leinenkugel, R., Deck, J., Huth, M., Ottinger, B., & Mack., (2019). The potential of open geodata for automated large-scale land use and land cover classification. *Remote Sensing, 11*, 2249. https://doi.org/10.3390/rs11192249.

Lin, C. H., Lin, B. Y., Lee, K. Y., & Chen, Y. C. (2015). Radiometric normalization and cloud detection of optical satellite images using invariant pixels. *ISPRS Journal of Photogrammetry, 106*, 107–111.

Liu, Y., Sheng, L., & Liu, J. (2015). Impact of wetland change on local climate in semi-arid zone of Northeast China. *Chinese Geographical Science, 25*(3), 309–320.

Lucas, L., Janssen, F., Frans, J.M., van der, W. (1994). Accuracy Assessment of Satellite Derived Land-Gover Data: A Review Photogrammetric Engineering & Remote Sensing, Vol. 60, No.4, April 1994, pp. 479–426. 0099 -11.72 I I 4/6 004-4 1 9$03.

Lu, D., Mausel, P., Brondizio, E., & Moran, E. (2004). Change detection techniques. *International Journal of Remote Sensing, 25*(12), 2365–2407.

Mack, B. P., Leinenkugel, C., & Kuenzer, S. D. (2017). A semi-automated approach for the generation of a new land use and land cover product for Germany based on landsat time-series and lucas in-situ data. *Remote Sensing Letters, 8*, 244–253. https://doi.org/10.1080/2150704x.2016.1249299.

Massetti, A., & Gil, A. (2020). Mapping and assessing land cover/land use and aboveground carbon stocks rapid changes in small oceanic islands' terrestrial ecosystems: A case study of Madeira Island, Portugal (2009–2011). *Remote Sensing of Environment, 239*, 111625.

Mohamed, S. A., & El-Raey, M. E. (2019). Land cover classification and change detection analysis of Qaroun andWadi El-Rayyan lakes using multi-temporal remotely sensed imagery. *Environmental Monitoring and Assessment, 191*, 229.

Mondal, M. S. N., Sharma, P. K., & Garg, M. K. (2016). Statistical independence test and validation of CA Markov land use land cover (LULC) prediction results. *The Egyptian Journal of Remote Sensing and Space Sciences, 19*(2), 259–272.

Mondal, A., Khare, D., Kundu, S., Mondal, S., Mukherjee, S., & Mukhopadhyay, A. (2017). Spatial soil organic carbon (SOC) prediction by regression kriging using remote sensing data. *The Egyptian Journal of Remote Sensing and Space Sciences, 20*, 61–70.

Nguyen, L. H., Joshi, D. R., Clay, D. E., & Henebry, G. M. (2020). Characterizing land cover/land use from multiple years of Landsat and MODIS time series: A novel approach using land surface phenology modeling and random forest classifier. *Remote Sensing of Environment, 238*, 111017. https://doi.org/10.1016/j.rse.2018.12.016.

Nitin, B., Kumar, M. D., Anuradha, S., & Pardha-Saradhi, P. (2014). Status of wetlands in India: a review of extent, ecosystem benefits, threats and management strategies. *Journal of Hydrology: Regional Studies, 2*, 1–19.

Omer, A.A. (1996). Geological, Mineralogical and Geochemical Studies on the Neogene and Quaternary Nile Basin Deposits, Qena-Assiut Stretch, Egypt. Ph.D. Thesis, South Valley University, Sohag, Egypt.

Pflugmacher, D., Rabe, A., Peters, M., & Hostert, P. (2019). Mapping pan-European land cover using landsat spectral-temporal metrics and the European LUCAS survey. *Remote Sensing of Environment, 221*, 583–595. https://doi.org/10.1016/j.rse.2018.12.001.

Rao, G. V., Kumar, A., Kumar, A. S., & Shashi, M. (2018). Spatiotemporal monitoring of shifting cultivation using landsat images: Soft classification approach. *Journal of the Indian Society of Remote Sensing, 46*, 1047–1052. https://doi.org/10.1007/s12524-018-0770-6.

Rawat, J. S., & Kumar., (2015). Monitoring land use/cover change using remote sensing and GIS techniques: A case study of Hawalbagh block, district Almora, Uttarakhand, India. *The Egyptian Journal of Remote Sensing and Space Sciences, 18*, 77–84.

Rebelo, L. M., Finlayson, C. M., & Nagabhatla, N. (2009). Remote sensing and GIS for wetland inventory, mapping and change analysis. *Journal of Environmental Management, 90*, 2144–2153.

Said, R. (1981). The Geological Evolution of the River Nile; Springer: New York, NY, USA.

Shalaby, A., & Tateishi, R. (2007). Remote sensing and GIS for mapping and monitoring land cover and land-use changes in the Northwestern coastal zone of Egypt. *Applied Geography, 27*(1), 28–41.

Solaimani, K., Arekhi, M., Tamartash, R., & Miryaghobzadeh, M. (2010). Land use/cover change detection based on remote sensing data (a case study; Neka Basin). *Agriculture and Biology Journal of North America*. https://doi.org/10.5251/abjna.2010.1.6.1148.1157,1.

Stehman, S. V., & Czaplewski, R. L. (1998). Design and analysis for thematic map accuracy assessment: fundamental principles. *Remote Sensing of Environment, 64*, 331–344.

Szuster, B. W., Chen, Q., & Borger, M. (2011). A comparison of classification techniques to support land cover and land use analysis in tropical coastal zones. *Applied Geography, 31*(2), 525–532.

Townshend and Justice. (1986). Analysis of the dynamics of African vegetation using the normalized difference vegetation index. International Journal of Remote Sensing, 7(11) 1435– 1445

Tassopoulou, M., Verde, N., Mallinis, G., Georgiadis, C., Kaimaris, D., & Patias, P. (2019). Demonstrating the potential of remote sensing to support Sustainable development goals implementation: Case studies over Greece sensing images. *Remote Sensing, 10*, 472.

USGS, (2019). EarthExplorer Website for Downloading Satellite Remote Sensing Data. Retrived 9 January 2020, from, https://earthexplorer.usgs.gov/.

Veldkamp, A., & Lambin, E. F. (2001). Predicting land-use change. *Agriculture, Ecosystems and Environment, 85*, 1–6.

Van, D. P. C. (1996). Unbiased estimates of class proportions from thematic maps. *Photogrammetric Engineering and Remote Sensing, 62*, 409–412.

Wang, F., Ge, Q., Yu, Q., Wang, H., & Xu, X. (2017). Impacts of Land-use and Land-cover Changes on River Runoff in Yellow River Basin for Period of 1956–2012. *Chinese Geographical Science, 27*(1), 13–24.

Yang, X., & Wen, X. (2011). Post classification comparison change detection of Guangzhou Metropolis, China. *Key Engineering Materials, 467*(469), 19–22. https://doi.org/10.4028/www.scientific.net/KEM.467-469.19.

Yin, Z. Y., Stewart, D. J., Bullard, S., & MacLachlan, J. T. (2005). Changes in urban built-up surface and population distribution patterns during 1986–1999: A case study of Cairo Egypt. *Computers, Environment and Urban Systems Environ, 29*(5), 595–616. https://doi.org/10.1016/j.compenvurbsys.2005.01.008.

Yohanis, K., & D'Huart, J. P. (2014). Assessment of the Present Distribution of the Forest Hog (Hylochoerusmeinertzhageni) in Ethiopia. *Journal of Mountain Ecology, 3*, 46–48.

Youssef, M. A., Ghallab, A,. (2007). Using Remotely sensed data, GIS and field investigation for preliminary consedrations of sustainable development West Qena area, Egypt.Assiut University Bulletin For Environmental Researches, 10(2).

Yuanbin, C., Hao, Z., Peng, Z., & Wenbin, P. (2016). Quantifying the impact of land use/land cover changes on the urban heat island: a case study of the natural wetlands distribution area of Fuzhou city China. *Wetlands, 36*(2), 285–298.

Zeng, Y. N., Wu, G. P., Zhan, F. B., & Zhang, H. H. (2008). Modeling spatial land use pattern using autologistic regression. *The International Archives of the Photogrammetry, Remote Sensing and Spatial Information Sciences, XXXVII*, 115–118.

Zhiliang, W., Zongming, W., Bai, Z., Chunyan, L., & Chunying, R. (2015). Impact of land use/land cover changes on ecosystem services in the Nenjiang River Basin, Northeast China.

Ecological Processes, *4*(1), 11. https://doi.org/10.1186/s13717-015-0036-y.

Zhou, Q., Li, B., & Kurban, A. (2008). Trajectory analysis of land covers change in arid environment of China. *International Journal of Remote Sensing, 29*(4), 1093–1107. https://doi.org/10.1080/01431160701355256.